

A development of SPH model for simulating surface erosion by impact(s) of single irregular-shaped particles

***Xiangwei Dong^{1,2}, G.R. Liu²**

¹College of mechanical and electronic engineering, China University of Petroleum (East China),
66 Changjiang Rd, Huangdao District, Qingdao, China

²CEAS-School of Aerospace Systems, University of Cincinnati,
2851 Woodside Dr, Cincinnati OH 45221, USA.

*Presenting author: dongxw139@163.com

†Corresponding author: dongxw139@163.com

Abstract

Modeling and studying the impact of single angular particles are very helpful in understanding the fundamental mechanisms of erosive wear. However, the majority of previous studies focused on well-defined symmetrical particles, which are not well representative of the abrasive particles. Hence, this study develops a mesh-free model based on the smoothed particle hydrodynamics (SPH) method to simulate impact(s) of single arbitrary-shaped particles on ductile material. A novel procedure is proposed to model the particle as a polygonal rigid body through measuring the corner vertices. The ductile material properties are modeled by using the Mie–Grüneisen equation of state and the Johnson–Cook model. Simulations are carried out by varying the initial input conditions and by using different types of angular particles. Common erosion mechanisms such as cutting, machining, ploughing, prying-off are successfully reproduced by the model. The predicted crater is compared with available experimental data, and good agreement has been achieved. The proposed SPH model and our present study could be useful in the study of erosive wear on the surface of metal devices that carries granular substances.

Keywords: smoothed particle hydrodynamics (SPH), arbitrary-shaped particles, ductile material, erosion mechanisms, erosive wear

Introduction

Studies on the impingement of single angular particles of known geometry are very helpful in understanding the fundamental mechanism of material removal in erosive wear. Through experimental and theoretical studies of single square particles (8mm), Hutchings [1] identified two types of cutting deformations: Type-1 cutting and Type-2 cutting (machining). Papini *et al.* observed that a rhombic particle (6.36mm) with backward spin can lead to a "prying-off" action, which is different from the machining action of square particles [2,3]. Winter and Hutchings [4] revealed that angular-type particles, at largely negative rake angles, could result in ploughing deformation, while the ploughing was generally accepted as the method by which spherical particles remove material [5].

However, the majority of known studies focused on well-defined symmetrical particles, such as square [1,6] and rhombic particles [3,7,8] (see Figure 1). One reason is that symmetrical particles are relatively easy to control in experiments. Nevertheless, computer models are not subject to this limitation. The rigid-plastic model developed by Papini and Spelt [9] was able to handle arbitrary-shaped

particles, but no relevant work was reported. In recent decades, numerical models based on the finite element method (FEM) or SPH method have been gradually used in the field of erosive wear [13,14,15,16] or similar fields (e.g. shot peening [17,18]). Papini first applied the FEM to simulate single rhombic particle impacting on a copper target [7]. Azimian employed a similar model to investigate the effect of incident parameters on the rebound kinematics and erosive craters [19]. However, large deformation of materials due to the impact of angular particles may lead to a mesh distortion problem [6], which is not conducive to the numerical stability. The SPH method, which is a mesh-free method, became more popular in recent. The relevant applications include simulation of single particle impact [6,8,20], particle embedment [21], and multiple and overlapping impacts [10,11]. In this study, an erosion model based on SPH method is developed to model the erosion process due to the impact(s) of angular particles.

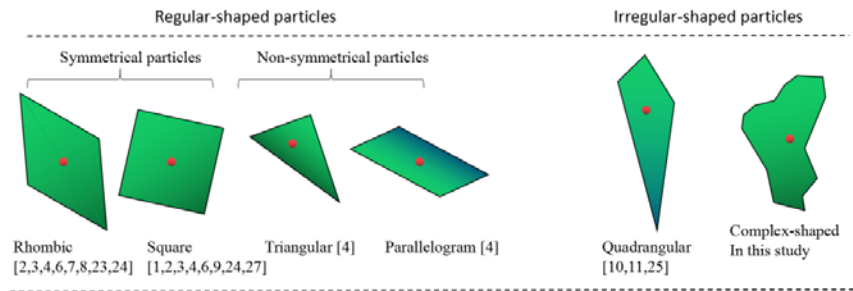


Figure 1. Several types of angular-type particles

This paper is organized into five sections. In section 2, the SPH model is introduced. The procedure to model an arbitrary-shaped particle is proposed. In section 3, the SPH model is validated by comparing the simulated results with the available experimental data. In section 4, the model is applied to simulate the impact(s) of single angular-type particles on OFHC copper target. Three irregular-shaped particles are selected from the SEM images of abrasive powder from the literature [22]. In section 5, the simulation results are analyzed.

Model description

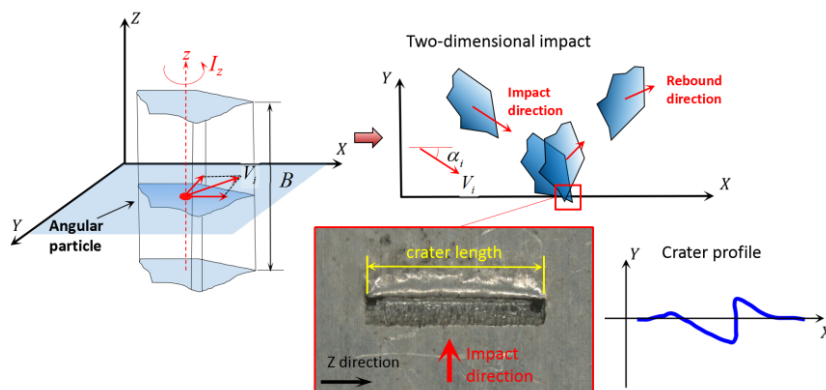
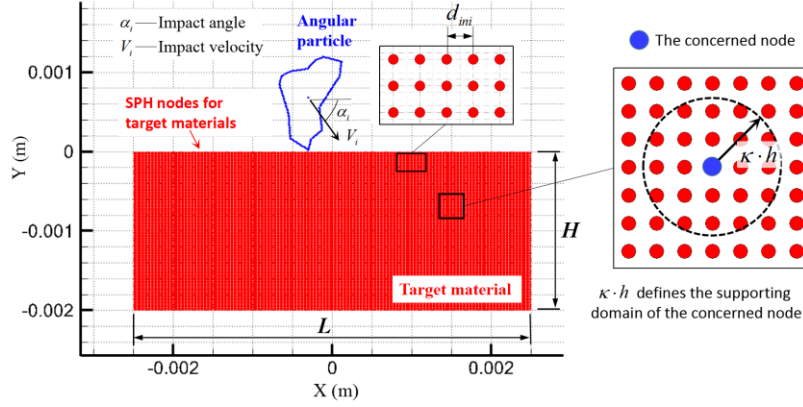


Figure 2. Coordinate system

This study is concerned with impact of single angular-type particle having constant thickness (B), given an initial impact velocity (V_i), an impact angle (α_i) and an initial orientation (θ_i). Referring to Figure 2, the impact and particle tumbling all occur in a single plane, the XY plane ($Z=0$). Therefore, the impact could be considered two dimensional. The surface of target materials is defined by $Y=0$.


Figure 3. SPH erosion model

The computing domain consists of two parts: the target block and the angular particle (see Figure 3). The target is considered as elastic-plastic material. The angular particle is treated as a rigid body. L is the length of the target block, H is the height of the target block. The target is expressed by a series of uniformly distributed SPH nodes, of which initial spacing is d_{ini} .

SPH equations for the target

The target is discretized by a set of SPH nodes, and each node represents a volume of material ($\Delta V_i = \frac{m_i}{\rho_i}$), carries the field information such as density (ρ_i), velocity (v_i), stress (σ_i) and so on. The following are the governing equations comprising mass and momentum conservation equations in SPH approximation form[24]:

$$\begin{cases} \frac{d\rho_i}{dt} = \rho_i \sum_{j=1}^N \frac{m_j}{\rho_j} (v_i^\beta - v_j^\beta) \cdot \frac{\partial W_{ij}}{\partial x_i^\beta} \\ \frac{dv_i^\alpha}{dt} = \sum_{j=1}^N m_j \left[\frac{\sigma_i^{\alpha\beta} + \sigma_j^{\alpha\beta}}{\rho_i \rho_j} - \Pi_{ij} \delta^{\alpha\beta} \right] \frac{\partial W_{ij}}{\partial x_i^\beta} + \frac{f_i^\alpha}{m_i} \end{cases} \quad (1)$$

Here, the subscript j represents the neighbor of i . N is the total number of neighboring nodes within the supporting domain, α and β are the indices for the Cartesian coordinates x and y , respectively. x^α is the position vector. $\sigma^{\alpha\beta}$ is the stress tensor, f^α is the external force. The term (Π_{ij}) is the artificial viscosity [31]. $W_{ij} = W(|\mathbf{x}_i - \mathbf{x}_j|, h)$, W is the weight, or kernel. A cubic spline kernel [25] is employed in this study.

The stress tensor $\sigma^{\alpha\beta}$ in Eq.(1) is normally divided into two parts: isotropic pressure p and deviatoric stress $\tau^{\alpha\beta}$, $\sigma^{\alpha\beta} = -p\delta^{\alpha\beta} + \tau^{\alpha\beta}$. The pressure is computed by using Mie-Grüneisen form of the equation of state [23]:

$$p = \frac{\rho_0 C_0^2 \eta \left(1 + \left(1 - \frac{\Gamma_0}{2} \right) \eta \right)}{(1 - (S_a - 1)\eta)} + \rho_0 \Gamma_0 e \quad (2)$$

where ρ_0 is the reference density of the target material, $\eta = \frac{\rho}{\rho_0} - 1$. e is the internal energy of unit mass. C_0 is the reference sound speed, Γ_0 is the Gruneisen coefficient, S_a is a linear Hugoniot slope coefficient.

The deviatoric stress ($\tau^{\alpha\beta}$) is estimated in the following equation [25]:

$$\frac{d\tau^{\alpha\beta}}{dt} = 2G \left(\dot{\varepsilon}^{\alpha\beta} - \frac{1}{3} \delta^{\alpha\beta} \dot{\varepsilon}^{\gamma\gamma} \right) + \tau^{\alpha\gamma} \cdot \dot{\gamma}^{\beta\gamma} + \tau^{\gamma\beta} \cdot \dot{\gamma}^{\alpha\gamma} \quad (3)$$

where G is the shear modulus of the concerned material, $\dot{\varepsilon}^{\alpha\beta} = \frac{1}{2} \left(\frac{\partial v^\alpha}{\partial x^\beta} + \frac{\partial v^\beta}{\partial x^\alpha} \right)$ is the strain rate tensor, $\dot{\gamma}^{\alpha\beta} = \frac{1}{2} \left(\frac{\partial v^\alpha}{\partial x^\beta} - \frac{\partial v^\beta}{\partial x^\alpha} \right)$ is the rotation rate tensor.

The materials are transitioned from elasticity to plasticity at the limitation of combined stress (σ_y , yield stress) according to von-Mise criterion. In this study, oxygen-free high thermal conductivity (OFHC) copper is selected as the target material. The purely empirical Johnson–Cook model [26] is adopted to model the viscoplastic behavior of copper target. The study of Banerjee shown Johnson–Cook model (for deviatoric behavior) combined with the Mie–Grüneisen equation (for hydrostatic behavior) work well for OFHC Copper[27]. The Johnson–Cook model associates the instantaneous yield stress (σ_y) with the initial yield stress (A), the equivalent strain (ε_{eff}^p), the equivalent strain rate ($\dot{\varepsilon}_{eff}^p$), and the temperature (T), expressed as,

$$\sigma_y = \left[A + B(\varepsilon_{eff}^p)^N \right] \left[1 + C \ln \left(\frac{\dot{\varepsilon}_{eff}^p}{\dot{\varepsilon}_0} \right) \right] \left[1 - \left(\frac{T - T_{ref}}{T_{melt} - T_{ref}} \right)^M \right] \quad (4)$$

where T_{melt} is melting temperature of concerned material, T_{ref} is reference temperature and $\dot{\varepsilon}_0$ is reference strain rate. A , B , C , N , and M are material dependent constants. The material parameters of OFHC Copper for Johnson-Cook equation and Mie–Grüneisen equation are taken from the literatures[26][28].

Rigid body equations and contact forces with SPH

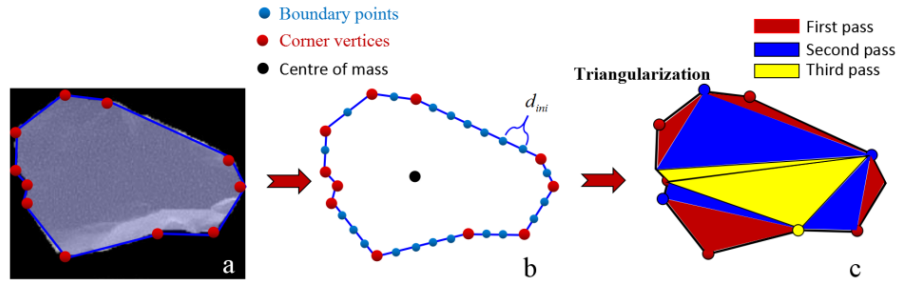


Figure 4. Description of an irregular-shaped particle through corner vertices and boundary points

As shown in Figure 4, an irregular-shaped particle is modeled as a polygon-shaped rigid body, which is described by the corner vertices of the actual particle. Boundary points are generated along the outline surface of the body using a fixed spacing. These boundary points are used to calculate the boundary normal vector. An array defined as $\text{Surface_List}(k, k+1, k-1)$ is established to store the boundary points (see Figure 5), where k is a boundary point, $k+1$ and $k-1$ are the adjacent points of k .

The motion of the rigid body is divided into two parts: translational velocity and rotational velocity. The following are the motion equations:

$$\frac{D\vec{X}_c}{Dt} = \vec{V}_c \quad \frac{D\vec{V}_c}{Dt} = \frac{\vec{F}_{tol}}{M} \quad (5)$$

$$\frac{D\vec{\Omega}_c}{Dt} = \frac{\vec{T}_{tol}}{I_z} \quad (6)$$

where \vec{V}_c , $\vec{\Omega}_c$, \vec{X}_c , M , I_z denote the translational velocity, the rotational velocity, the position vector of the centre of mass, the mass and the moment of inertia of the rigid body. $\vec{F}_{tol} = -\sum_{j=1}^{N_c} (\vec{f}_{nj} + \vec{f}_{\tau j})$ and $\vec{T}_{tol} = -\sum_{j=1}^{N_c} \vec{f}_{jc} \times (\vec{x}_j - \vec{X}_c)$ are the contact force and moment acting on the rigid body. N_c is the number of SPH points interacting with the rigid body, \vec{f}_{nj} is the normal force acting on the SPH point j , $\vec{f}_{\tau j}$ is the tangential force acting on the SPH point j .

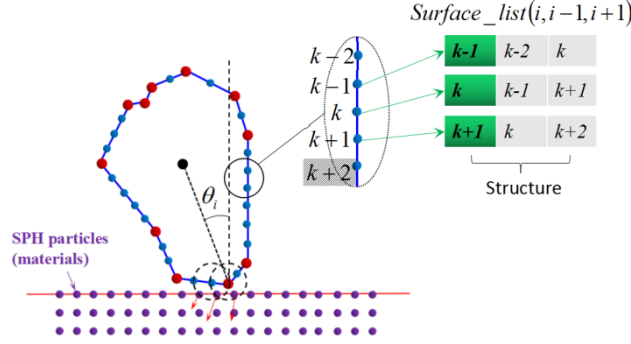


Figure 5. Boundary points for the angular particle

For the rigid body, the boundary normal vector \vec{n}_k at an arbitrary boundary point k can be calculated by the following equation:

$$\vec{n}_k = \pm \left(\frac{y_{k+1} - y_{k-1}}{|\vec{x}_{k+1} - \vec{x}_{k-1}|}, -\frac{x_{k+1} - x_{k-1}}{|\vec{x}_{k+1} - \vec{x}_{k-1}|} \right) \quad (7)$$

where $\vec{x}_{k+1} = (x_{k+1}, y_{k+1})$, $\vec{x}_{k-1} = (x_{k-1}, y_{k-1})$.

Once the boundary normal vectors are determined, the next is to evaluate whether contact occurs or not. In this study, the following criterion is used:

$$p = \sqrt{h_{ik}^2 - r_{ik}^2 + (\vec{n}_{av} \cdot \vec{r}_{ik})^2} - |\vec{n}_{av} \cdot \vec{r}_{ik}| > 0 \quad (8)$$

where p is the penetration, $h_{ik} = \frac{h_i + h_k}{2}$, h_i and h_k are the smoothing lengths of SPH node i and rigid body point k , \vec{n}_{av} is the average normal vector, $\vec{n}_{av} = \frac{\vec{n}_k - \vec{n}_i}{2}$, $\vec{r}_{ik} = \vec{r}_k - \vec{r}_i$. Thereby, the contact force is function of penetration (if the criterion in Eq.(8) is met) and expressed as follows,

$$\vec{f}_n = (1 - \chi) \cdot \left\{ \max \left(\frac{m_i p}{\Delta t^2}, \frac{2m_i c_i p}{\Delta t \cdot |\vec{r}_{ik}|} \right) \right\} \quad (9)$$

where χ defines the extent of the residual penetration, and $\chi=0$ means no penetration is allowed, m_i is the mass of SPH point i .

According to basic principles presented above, a SPH procedure is established based on the SPH code written in Fortran[24].

Model validation using scaled-up particles

The model is validated by reproducing the experiment in reference [7]. The scaled-up rhombic particles (side length 5.46mm) were used to impact on OFHC copper target. The model parameters are $V_i = 85\text{m/s}$, $\alpha_i = 50^\circ$, $\theta_i = 50^\circ$. In Figure 6(a), the predicted crater profile is compared with the measured result. It can be seen that not

only the crater shape but also the dimensions are in good agreement with the measured data. The predicted particle trajectory (see Figure 6 (b)) shows that backward impact occurs. As observed by the experiment, the backward impact leads to two craters on the surface: a primary crater and secondary crater, this phenomenon is also well reproduced by the model. The ability of the model on accurately predicting the material deformation is verified.

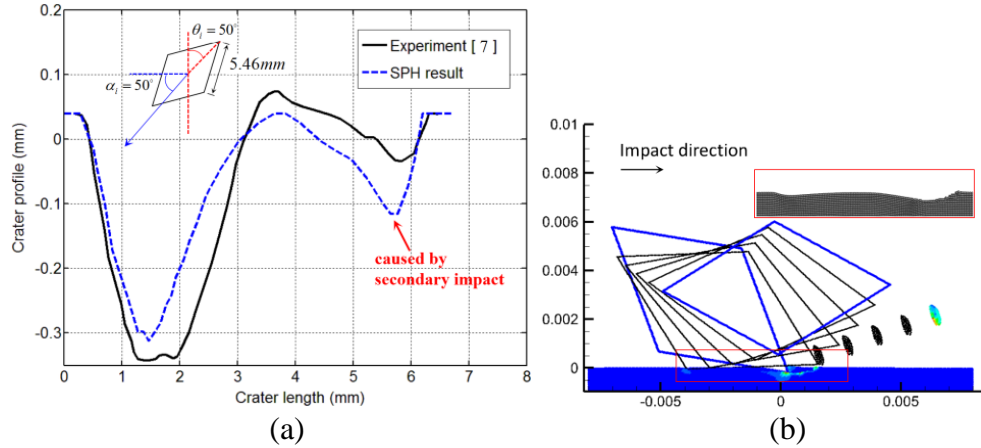


Figure 6. Backward impact results in chip separation of the material. (a) crater profiles (b) particle trajectory

Particles used for simulation

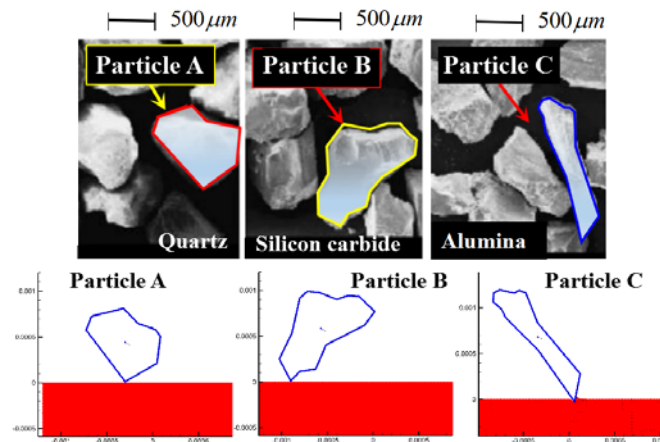


Figure 7. Irregular-shaped particles used for simulation (Top: images are cited from reference [22]; bottom: SPH models)

Figure 7 shows the images of abrasive powder (quartz, silicon carbide and alumina) obtained by scanning electron microscopy (SEM) in the literature[22]. It was observed that alumina particles are more angular than quartz and silicon carbide. The average shape factor of alumina particles is lowest as 0.3695 whereas it is 0.7195 and 0.4699 for quartz and silicon carbide particles. Therefore, we pick a particle from each type of powder for numerical simulation, they are particle A (quartz), particle B (silicon carbide), particle C (alumina), respectively. The corner vertices are measured, and the SPH models are built (see Figure 7). The hardness of the particles is much higher than OFHC copper target with a Brinell hardness of 26 [7], which meet the requirement of rigid-plastic assumption.

The parameters for single angular-type particle are divided into two categories (see Figure 8): one is defined on the center of mass, and the other is defined on the most

downstream vertex (the impacting vertex). The initial orientation (θ_i) is defined as the angle between the centroid line and the vertical direction (Y axis). Figure 8 (b) shows the parameters defined on the most downstream vertex. Three parameters, including the rake angle (θ_{rake}), the offset-angle of centroid (γ) and the angularity (A), are defined. The rake angle (θ_{rake}) is the angle between the leading edge of the particle and the vertical direction.

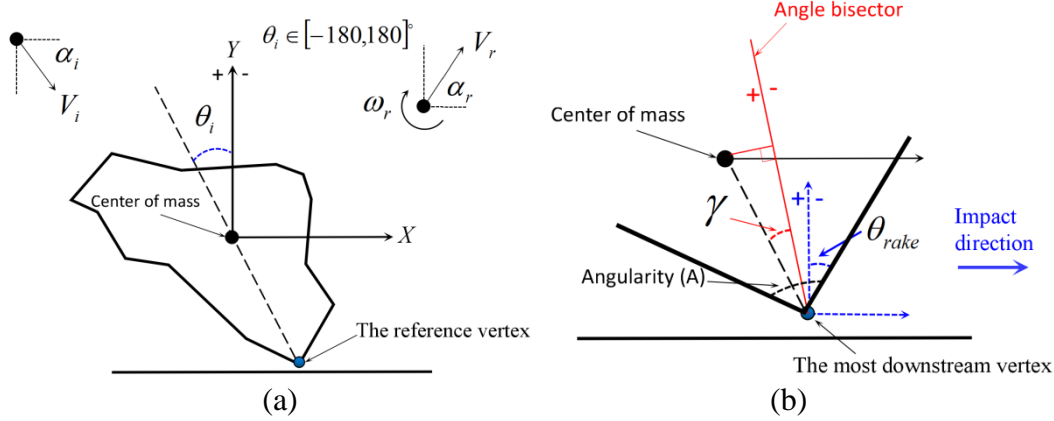


Figure 8. Definitions of parameters (a) parameters defined on the center of mass, (b) parameters defined on the most downstream vertex

Previous studies about symmetrical particles shown that θ_{rake} has a significant effect on the mechanism of deformation through influencing the tumbling behavior of the particle[1,3]. The angularity of the impacting vertex is also an important factor influencing the deformation mechanism[2]. Besides, Winter and Hutchings [4] qualitatively analyzed the influence of location of center of mass on particle rotation, and believed that it introduces a further factor affecting the pattern of deformation. For a given shape of the particle, the initial orientation of the particles influences the erosion process through changing the values of three parameters (θ_{rake} , A , γ).

Results and discussion

In order to investigate the erosion dependency on particle orientation, the impact angle and impact velocity are fixed at 30° and 100m/s , and the initial orientation (θ_i) is varied from -180° to 180° with an interval of 30° .

Surface morphology

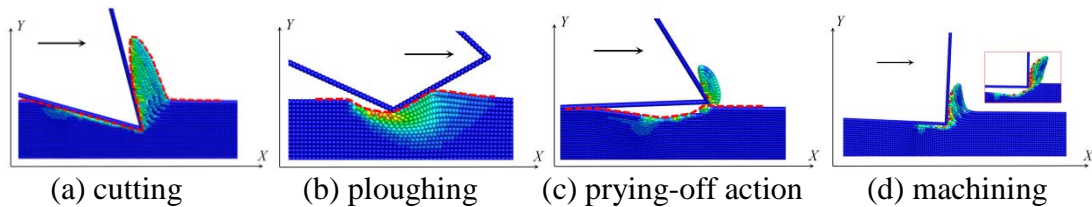


Figure 9. Impact craters predicted by the SPH model.

The model is able to reproduce the entire impact process. It allows tracking the motion of the particle, so that the rebound parameters can be obtained. The mechanism of deformation can be evaluated through the impact craters (see Figure 9). Impact craters for typical mechanisms, such as cutting (Figure 9 (a)), ploughing (Figure 9 (b)), machining (Figure 9 (c)) and prying-off action (Figure 9 (d)) are successfully reproduced by the model.

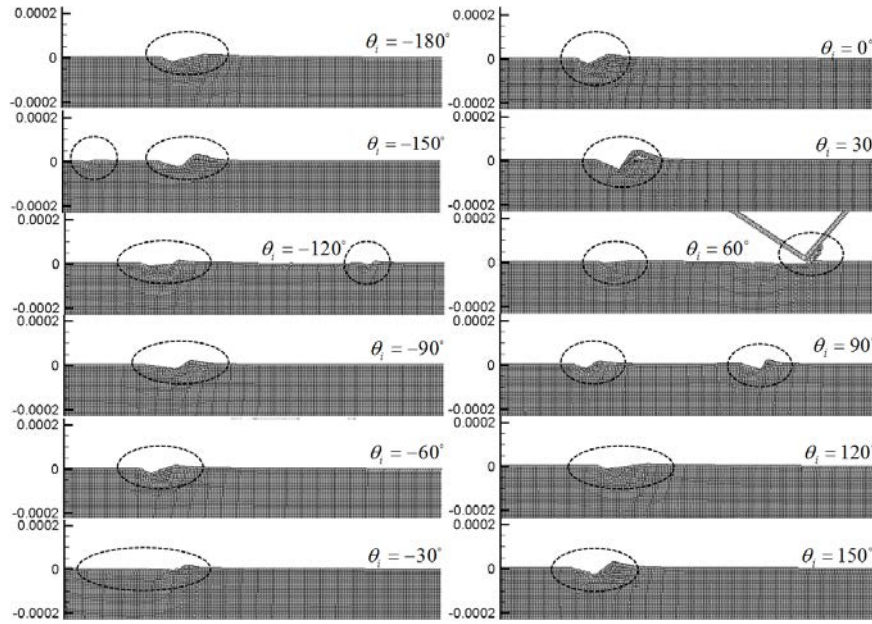


Figure 10. Predicted surface morphology due to impacts of particle-A (the ellipses mark the impact craters, and two or three ellipses means that the multi impacts occur)

When initial orientations of particle A are adjusted from -180° to 180° , the rake angle (θ_{rake}) varies in the range of $-83.88^\circ \sim -30.08^\circ$. The rake angles of particle A are more negative than that of the other two particles B and C, thus particle-A is more likely to result in ploughing. For particle-A, as shown in Figure 10, all 12 simulated cases cause ploughing deformation except the data point 9 (at $\theta_i = 60^\circ$). The only cutting deformation is caused by the secondary impact, not the primary impact.

Compared to particle-A, particle-B is more angular and has a wider range of rake angles involving positive values. A positive rake angle tends to result in cutting deformation [1]. For example, at $\theta_i = 30^\circ$ and -90° , the rake angles of particle B are 15.7° and -14.22° respectively, and cutting deformations are observed. The former is machining action (Type-2 cutting), the latter is Type-1 cutting action (see Figure 11).

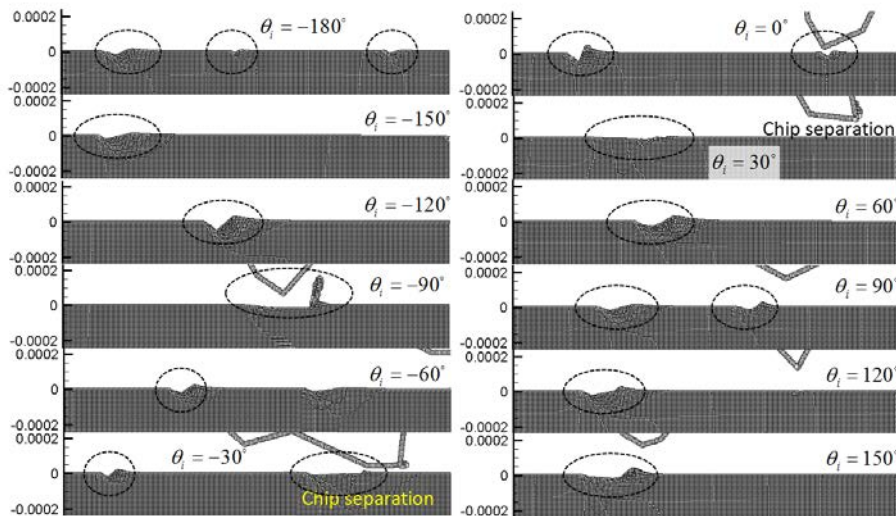


Figure 11. Predicted surface morphology due to impacts of particle-B

Particle-C has the largest slender ratio and more angular ($A_{min} = 46.49^\circ$) than particle A and particle B. By comparing the energy loss (δ) of the three particles, particle C corresponds to the highest level of energy loss. In particular, 11/12 of the data points of particle C have $\delta > 0.5$, especially when θ_i is between 60° and 90° , the values are very close to 1. Taking $\theta_i = 0^\circ, 30^\circ$ and 60° for example, Figure 12 shows the crater profiles at three initial orientations, at which the same impacting vertex is used ($A = 46.49^\circ$). It can be seen that the deformation mechanism changes from ploughing to Type 1 cutting with the increase of the rake angle.

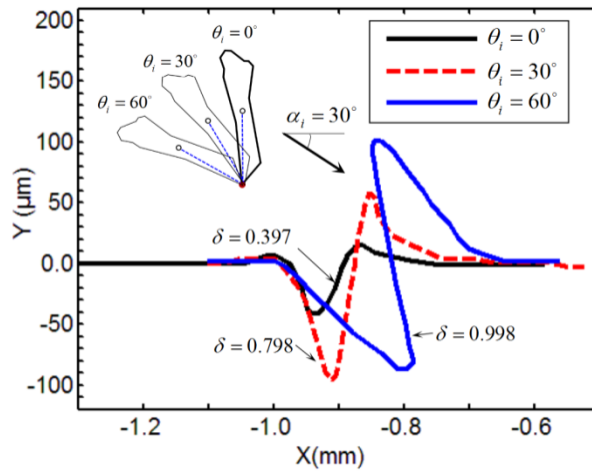


Figure 12. Crater profiles at $\theta_i = 0^\circ, 30^\circ$ and 60° (Particle C)

Particle kinematics

The particle trajectories can be obtained by superimposing the particle locations at different moments. Figure 13 (a) and (b) show the predicted trajectories of the particles, from which one can easily identify the tumbling direction of the particle. Besides, the time history of the angular velocities of the particles is obtained, which helps to understand the tumbling behavior (see Figure 14).

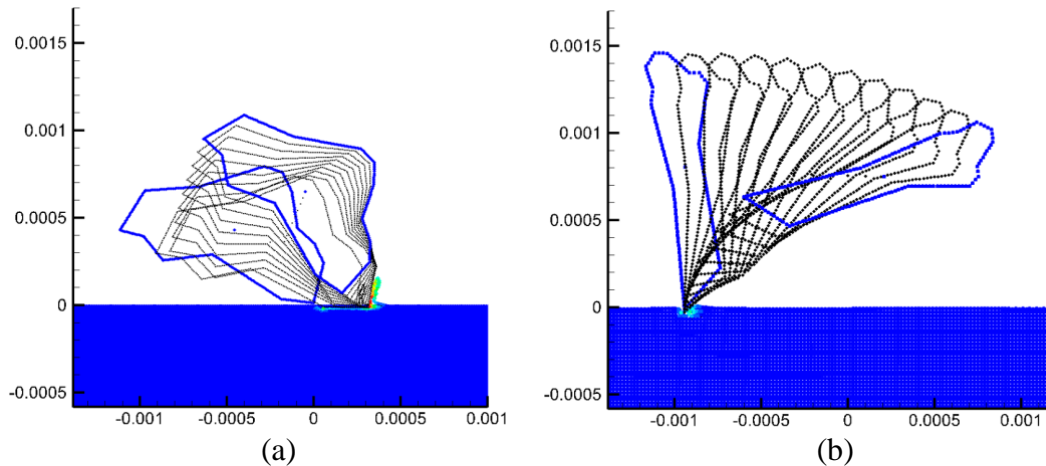


Figure 13. The predictions of motion trajectory of (a) particle B at $\theta_i = -90^\circ$, (b) particle C at $\theta_i = 0^\circ$

Figure 13 (a) and (b) show the forward impacts of particle B and particle C. For particle B, as shown in Figure 14, there exists a transition point from backward to forward (positive value means backward rotation). While for particle C, the particle keeps tumbling forwards from the beginning to the end.

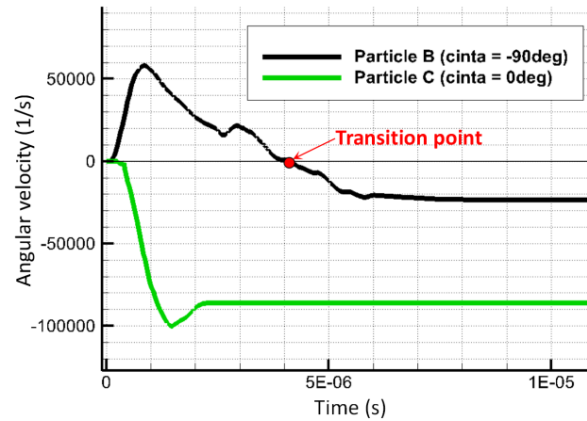


Figure 14. The predictions of time history of the angular velocities of the particles

An angular particle rotating forward can produce two or three impacts, which was defined as "forward and multiple impact"[3]. Taking Particle-A for example (see Figure 15), the first impact occurs at a highly negative $\theta_{rake} = -82.9^\circ$ and at a negative $\gamma = -25.43^\circ$, which makes the particle rotate forwards. Then, the sharper vertex contacts the surface at a relatively positive $\theta_{rake} = -9.8^\circ$ and a positive $\gamma = 11.49^\circ$ for the second impact, resulting in the cutting deformation of the surface.

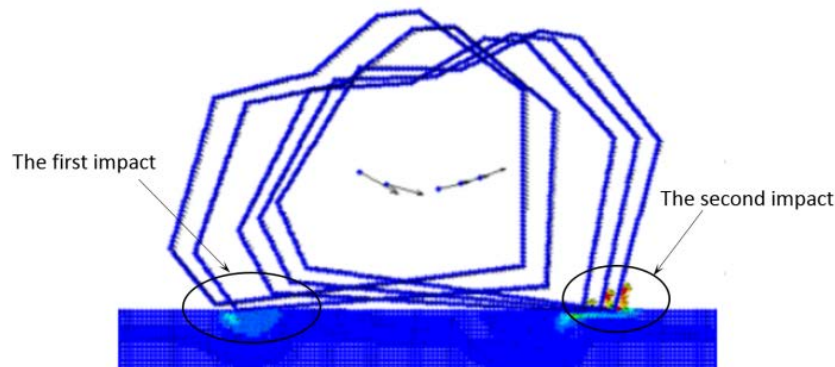


Figure 15. Illustration of "forward and multiple impacts"

Conclusions

This paper proposes a modeling procedure to simulate angular-type particles impacting on ductile surfaces using SPH method. An arbitrary-shaped particle is modeled as a polygonal rigid body using measured corner vertices. Boundary points are generated along the outline surface of the rigid body, which helps to detect the contact and to enforce the contact condition. Through this modeling procedure, the shape features of the abrasive particles, such as shape factor, distribution of angularities, position of centre-of-mass, etc, can be retained. Simulations are conducted for several irregular-shaped particles over a wide range of initial orientations from -180° to 180° , at a constant impact angle ($\alpha_i = 30^\circ$) and impact velocity ($V_i = 100\text{m/s}$). As observed by simulations, the probability of occurrence of cutting behavior increases as the shape factor increases. However, the type of erosion mechanism depends mainly on the three parameters at the moment of impact, which are the rake angle (θ_{rake}), the angularity of the impacting vertex (A), and offset-angle of centroid (γ). For a given shape of the particles, the three parameters are determined by the initial orientation of the particles. When the initial orientation

(θ_i) changes from -180° to 180° , the impact(s) of an irregular-shaped particle may cause either ploughing or cutting deformation.

The application of the model on three-dimensional case is easy to be realized without too much additional efforts, which will be considered in the future work.

References

- [1] I.M. Hutchings, Deformation of metal surfaces by the oblique impact of square plates, *Int. J. Mech. Sci.*19 (1977)45–52.
- [2] Papini M, Dhar S. Experimental verification of a model of erosion due to the impact of rigid single angular particles on fully plastic targets [J]. *International Journal of Mechanical Sciences*, 2006, 48(5):469-482.
- [3] S. Dhar, T.Krajac, D. Ciampini, M. Papini, Erosion mechanisms due to impact of single angular particles, *Wear* 258(2005): 567–579.
- [4] Winter R E, Hutchings I M. Solid particle erosion studies using single angular particles[J]. *Wear*, 1974, 29(2): 181-194.
- [5] I.M. Hutchings, N.H. Macmillan, D.G. Rickerby, Further studies of the oblique impact of a hard sphere against a ductile solid, *Int. J. Mech. Sci.*23 (1981) 639–646.
- [6] M. Takaffoli, M. Papini. Material deformation and removal due to single particle impacts on ductile materials using smoothed particle hydrodynamics [J]. *Wear*, 2011, 274(3):50-59.
- [7] M. Takaffoli, M.Papini, Finite element analysis of single impacts of angular particles on ductile targets, *Wear* 267(2009): 144–151.
- [8] Dong X, Li Z, Liu G, et al. Numerical Study of Impact Behaviors of Angular Particles on Metallic Surface Using Smoothed Particle Hydrodynamics [J]. *Tribology Transactions*, 2016: 1-18.
- [9] M. Papini, J.Spelt, Impact of rigid angular particles with fully-plastic targets Part I: analysis, *Int. J. Mech. Sci.* 42(2000)991–1006.
- [10]Takaffoli M, Papini M. Numerical simulation of solid particle impacts on Al6061-T6 part I: Three-dimensional representation of angular particles[J]. *Wear*, 2012, 292–293(29):100-110.
- [11]Takaffoli M, Papini M. Numerical simulation of solid particle impacts on Al6061-T6 Part II: Materials removal mechanisms for impact of multiple angular particles[J]. *Wear*, 2012, 296(s 1–2):648–655.
- [12]Brown J R, Chappell P J C, Egglestone G T, et al. A gas-gun facility for material impact studies using low-velocity, low-mass projectiles[J]. *Journal of Physics E: Scientific Instruments*, 1989, 22(9): 771.
- [13]M. Junkar, B.Jurisevic, M.Fajdiga,M.Grah, Finite element analysis of single-particle impact in abrasive water jet machining, *Int. J. Impact Eng.* 32(2006) 1095–1112.
- [14]K. Shimizu,T.Noguchi,H.Seitoh,M.Okada,Y.Matsubara,FEM analysis of erosive wear, *Wear* 250(2001)779–784.
- [15]M. ElTobgy, E.Ng, M.Elbestawi, Finite element modeling of erosive wear, *Int. J. Mach. Tools Manuf.*4 5(2005)1337–1346.
- [16]Liu Z G, Wan S, Nguyen V B, et al. A numerical study on the effect of particle shape on the erosion of ductile materials[J]. *Wear*, 2014, 313(1): 135-142.
- [17]Meguid S A, Shagal G, Stranart J C. 3D FE analysis of peening of strain-rate sensitive materials using multiple impingement model[J]. *International Journal of Impact Engineering*, 2002, 27(2): 119-134.
- [18]Levers A, Prior A. Finite element analysis of shot peening[J]. *Journal of Materials Processing Technology*, 1998, 80: 304-308.
- [19]Azimian M, Schmitt P, Bart H J. Numerical investigation of single and multi impacts of angular particles on ductile surfaces[J]. *Wear*, 2015, 342: 252-261.
- [20]Dong X W, Liu G R, Li Z, et al. A smoothed particle hydrodynamics (SPH) model for simulating surface erosion by impacts of foreign particles[J]. *Tribology International*, 2016, 95:267-278.
- [21]Hadavi V, Papini M. Numerical modeling of particle embedment during solid particle erosion of ductile materials[J]. *Wear*, 2015, 342: 310-321.
- [22]Desale G R, Gandhi B K, Jain S C. Effect of erodent properties on erosion wear of ductile type materials[J]. *Wear*, 2006, 261(7):914-921.
- [23]Randies PW, Libersky LD. Smoothed particle hydrodynamics: some recent improvements and applications. *Comput Method Appl Mech Eng.* 1996;139:375–408.
- [24]G.R. Liu, M.B. Liu. (2004), “Smoothed particle hydrodynamics: A meshfree particle method,” World Scientific, Singapore, 2004.
- [25]Monaghan, J. J., Lattanzio. J. C., A refined particle method for astrophysical problems, *Astronomy and Astrophysics*, 149 (1) (1985),135–143.

- [26] Johnson G R, Cook W H. Fracture characteristics of three metals subjected to various strains, strain rates, temperatures and pressures[J]. *Engineering fracture mechanics*, 1985, 21(1): 31-48.
- [27] Banerjee B. An evaluation of plastic flow stress models for the simulation of high-temperature and high-strain-rate deformation of metals[J]. *Physics*, 2005, 21:129-134.
- [28] Macdonald R A, Macdonald W M. Thermodynamic properties of fcc metals at high temperatures[J]. *Physical Review B*, 1981, 24(4):385-386.

Biography



Xiangwei Dong received his Ph.D. from China University of Petroleum(East China), in 2017. He is currently a Postdoctoral Fellow at China University of Petroleum (East China), China.

He was a visiting scholar at University of Cincinnati (USA), from 2013–2015. Representative papers: [1] X.W. Dong, G.R. Liu, Li Z, et al. *A smoothed particle hydrodynamics (SPH) model for simulating surface erosion by impacts of foreign particles*[J]. *Tribology International*, 2015, 95:267–278. [2] X.W. Dong, Zengliang Li, G.R. Liu, et al. *Numerical Study of Impact Behaviors of Angular Particles on Metallic Surface using Smoothed Particle Hydrodynamics*[J]. *Tribology Transactions*, 2016:00-00. [3] X.W. Dong, Zengliang Li, Zhang Q, et al. *Analysis of surface-erosion mechanism due to impacts of freely rotating angular particles using smoothed particle hydrodynamics erosion model*[J]. *Proceedings of the Institution of Mechanical Engineers, Part J: Journal of Engineering Tribology*, 2017: 1350650117700750.

感谢和祝福语



我是 2013 年至 2015 年在辛辛那提大学刘老师的实验室 (G.R Lab) 进行了为期两年的学术访问，主要从事 SPH 方法以及基于 SPH 方法的冲蚀模型研究。在两年的时间里，刘老师给了我很多帮助，是我科研道路上的启发人，我博士论文里的主要工作正是在这两年的访学期间里完成的。刘老师严谨的治学态度和对科研执着

的追求也深深的影响了我。在这里首先祝刘老师 60 岁生日快乐，在今后的日子里，身体健康。附上一张照片，是刘老师在 2016 年夏天访问我的母校中

国石油大学（华东）时的合影。希望刘老师永远年轻，再次感谢您对计算力学发展所做出的巨大贡献，感谢您对我科研生涯的帮助。